Novel 3D printable bio-based and biodegradable poly(3-hydroxybutyrate-co-3-hydroxyhexanoate) microspheres for selective laser sintering applications

Materials Today Sustainability 22 (2023) 100379

Contents lists available at ScienceDirect

Materials Today Sustainability

journal homepage: https://www.journals.elsevier.com/materials-today-sustainability

Novel 3D printable bio-based and biodegradable poly(3-hydroxybutyrate-*co*-3-hydroxyhexanoate) microspheres for selective laser sintering applications

A. Giubilini [a, b, *], G. Colucci [b, c, d], G. De Trane [c], F. Lupone [c, d], C. Badini [c, d], P. Minetola [a, b], F. Bondioli [b, c, d], M. Messori [b, c, d]

[a] Department of Management and Production Engineering (DIGEP), Politecnico di Torino, Corso Duca Degli Abruzzi 24, 10129 Torino, Italy
[b] Integrated Additive Manufacturing Centre (IAM@PoliTO), Politecnico di Torino, Corso Duca Degli Abruzzi 24, 10129 Torino, Italy
[c] Department of Applied Science and Technology (DISAT), Politecnico di Torino, Corso Duca Degli Abruzzi 24, 10129 Torino, Italy
[d] National Interuniversity Consortium of Materials Science and Technology (INSTM), Via G. Giusti 9, 50121 Firenze, Italy

ARTICLE INFO

Article history:
Received 14 October 2022
Received in revised form
2 March 2023
Accepted 3 March 2023
Available online 17 March 2023

Keywords:
Poly(3-hydroxybutyrate-*co*-3-hydroxyhexanoate)
Biopolymers
Selective laser sintering
Additive manufacturing
3D printing
Microspheres
Emulsion solvent evaporation

ABSTRACT

Selective laser sintering (SLS) has become the most popular additive manufacturing process due to its high accuracy, productive efficiency, and surface quality. However, currently there are still very few commercially available polymeric materials suitable for this technique. This research work focused on the fabrication and characterization of bio-based and biodegradable microspheres obtained by oil-in-water emulsion solvent evaporation, starting from a poly(3-hydroxybutyrate-*co*-3-hydroxyhexanoate) (PHBH) biopolymer matrix. First, the fabrication parameters were optimized to improve the morphological, thermal, and flowability properties of the synthetized microspheres. Once the best production conditions were established, the PHBH microspheres were further used to study their effective 3D printability on an SLS 3D printer using geometries varying from simple shapes to architectures with more complex internal patterns. The results of this research revealed that PHBH has promising applicability for the SLS technique. This study undertook the first step toward broadening the range of polymeric materials for this additive manufacturing technology. These findings will contribute to a greater and wider dissemination of the SLS technique in the future, as well as they will bring this manufacturing process closer to applications, such as the biomedical sector, where the use of biodegradable and biocompatible materials can add value to the final application.

1. Introduction

Since its appearance on the international scene, additive manuanufacturing (AM) has been revolutionizing all sectors in which it found application [1]. Compared to traditional manufacturing processes, AM shows many significant advantages that effected its affirmation and fortune in the market, such as higher freedom in design [2], weight reduction [3], prototyping, and modeling function [4], and a reduced time to market [5]. The KBV Market Research and Consulting Company foresees that the Global Additive Manufacturing Market size will reach $44.6 billion by 2028, rising at a market growth of almost 20% compounded average growth rate during the forecast period [6]. Roland Berger Strategy Consultants identified machine sales as the major driver of market growth in the recent future. And, as an indication, they recorded those sales of professional polymer AM machines, priced above 5000 €, have experienced an annual growth rate of 13% since 2007 [7]. The market trend suggests that the AM industry is in great and steady development, but there are still several aspects that need to be investigated. For this reason, both the academic and the industrial world are exploring new frontiers of AM, addressing the topic from different points of view, such as the development of innovative materials [8], the increase of dimensional accuracy [9], or the definition of optimized processing parameters [10,11]. The polymer AM technologies can be mainly divided into extrusion-based, powder bed fusion, and vat photopolymerization. The former 3D printing approach is the most popular and widespread because of its technological straightforwardness, relatively inexpensive

* Corresponding author.
E-mail address: alberto.giubilini@polito.it (A. Giubilini).

https://doi.org/10.1016/j.mtsust.2023.100379

equipment and material costs [12]. Nevertheless, a much higher surface quality, as well as greater printing accuracy, can be achieved with the other techniques.

For example, selective laser sintering is an AM technology that employs a laser to selectively melt polymer-based powder particles by scanning cross-sections of a 3D structure, such as an STL file, on the surface of a powder bed. The laser sintering process consists of three main phases: pre-heating, building, and cooling [13]. The pre-heating phase involves warming up the machine and polymeric powder to temperatures just below the melting point of the material, using a set of heaters placed above the build chamber. The building phase involves selectively heating the polymeric powder using a laser beam to melt the particles according to the geometry of the part to be printed. When a layer is completed, the building platform is lowered by one-layer thickness, and new material is spread by a roller, and the process is reiterated until the part is finished [14,15]. Finally, the third stage requires the cooling and solidification of the 3D-printed final component. At the end of the building process, the 3D-printed object is surrounded by loose powder inside the printing bed. This excess powder is removed and eventually reused for the next job [13]. Moreover, SLS does not require structural support for printing parts with overhanging features due to the self-supporting ability of the loose powders in the printing bed. However, post-processing is often necessary for a better surface finish [13]. The quality of the 3D-printed geometries greatly depends on the powder particle size, laser power, and scan speed as well as the thermo-physical properties of the powders. As a matter of fact, SLS requires good flowability of the powder during spreading before laser sintering, and this critically depends on the particle shape. Henceforth, having spherical particles allows for control over the final packing and size uniformity, ensuring better prediction of material behavior and enhanced repeatability [16–20].

To date, one drawback of this technique is the extremely limited range of commercially available polymer powders, namely polyamides (PA11, PA12, PA6) [16–18], polystyrene [19], and thermoplastic elastomers [20]. However, Data Bridge Market Research foresees that the global SLS market will exhibit a compounded average growth rateof more than 23% for the period 2022–2029 [21], and for such a market expansion, a great demand and receptive capacity for new polymer micro-powders can surely be expected.

In recent years, one of the biggest environmental issues that we are facing as a global society is plastic pollution with its social, financial, and ecological impacts [21,22]. Although most of the produced plastic is still represented by petroleum-based polymers, the development of suitable alternatives is a key action to achieve a sustainable future [23]. One promising replacement for traditional plastic is the use of biopolymers, whose demand and production on a global scale are expected to increase in the next 5 years, by more than 200% [24].

Biopolymers are categorized according to their origin and their end-of-life. In fact, if they derive, in whole or in part, from biomass resources, they are named as bio-based, and if they can be used as a carbon source by microorganisms and converted into CO_2, biomass and water, they are defined as biodegradable.

All polymers that possess at least one of these two properties are called biopolymers, but those which possess both, such as polyhydroxyalkanoates (PHAs) or cellulose-derived materials, are the most attractive and investigated [25]. The fields of application for biopolymers are varied and expanding, e.g. they range from packaging [26] to agriculture [27], from textile [28] to energy sectors [29,30], as well as the biomedical one [31,32].

Among biopolymers, PHAs have recently gained great attention from academic and industrial scientists due to their biodegradability under different conditions. Although the most promising results were obtained under industrial composting conditions, some PHAs were demonstrated to be compostable also under home conditions. The wide variety of PHAs copolymers depends on the differences in the bacterial strain and fermentation conditions selected for the bioengineered PHAs production, and these differences are reflected on the final properties, such as ductility, processability, or impact resistance [33]. Among these copolymers, the most investigated are poly(3-hydroxybutyrate-*co*-3-hydroxyvalerate) (PHBV) and poly(3-hydroxybutyrate-*co*-3-hydroxyhexanoate) (PHBH). PHBH is an aliphatic polyester, naturally synthesized by bacterial fermentation, under unbalanced growth conditions, which is both bio-based and biodegradable. Compared to PHB and PHBV, PHBH shows a wider processing window with better thermal stability and lower brittleness [33].

According to the authors' best knowledge, many studies are reported in the literature regarding the use of PHBV, as polymer matrix in composites for SLS, especially for application in the biomedical field [34–38]. On the contrary, the application of PHBH biopolymer for SLS AM applications is still extremely limited, and in any case, no previous research work had focused on this topic. For all these reasons, it is extremely challenging to expand knowledge in this specific area, as well as aiming to broaden the window of possible polymeric materials that can be processed by SLS AM process.

In this study, PHBH microspheres were first prepared through an emulsion solvent evaporation method, slightly modifying Duan's previously published methodology for PHBV [34]. Then, the powder obtained was characterized from the morphological, physical, and thermal points of view, and used as feedstock for an SLS 3D printer, to produce final objects that have the added value of combining the advantages of AM along with the bio-origin and biodegradability of the polymer material used.

The article paved the way for the expansion of the current material palette for SLS, thus contributing to develop the widespread use of this AM technique, using an environmentally friendly biopolymer, which we believe can be commercially accessible in the near future. The importance and novelty of this approach lies in the combination of the advantages of SLS 3D printing, for the production of customized solutions, along with the bio-origin, ecological sustainability, and biodegradability of the polymeric material used.

2. Material and methods

2.1. Materials

PHBH containing 11 mol % of 3-hydroxyhexanoate monomer was provided by MAIP Group (MAIP srl, Settimo Torinese, Italy) in pellet form with a density of 1.22 g/cm^3 and an Melt Flow Index (MFI) of 3 g/10 min, calculated according to standard India Standard Organization 1133-2 at 170 °C and with a mass of 5 kg, as reported by the supplier datasheet. Poly (vinyl alcohol) 8–88 and chloroform were purchased from Merck (Merck KGaA, Darmstadt, Germany) and used as received without further purification.

2.2. Fabrication of PHBH microspheres

PHBH microspheres were prepared using an oil-in-water (O/W) emulsion solvent evaporation method, modifying a previously published method [34]. PHBH pellets were dissolved in chloroform (oil phase, O) and then added drop-by-drop to an aqueous solution of poly (vinyl alcohol) (water phase, W). Different concentrations of

the single O and W phases, as well as their emulsion ratio, were tested. All the experimented formulations are enlisted in Table 1.

The resulting emulsion was kept under magnetic stirring at 700 rpm and room temperature until the solvent was completely evaporated. The obtained microspheres were filtered, washed several times with distilled water, and oven-dried at 40 °C overnight. Subsequently, the powder was collected and sieved to ensure a microsphere size of less than 100 μm.

A schematic representation of the micro-powder fabrication is shown in Fig. 1.

2.3. Characterization of PHBH microspheres

2.3.1. Scanning electron microscopy

The morphology of the PHBH microspheres was investigated by a Phenom™ XL G2 Desktop Scanning Electron Microscope (Thermo Fisher Scientific, Waltham, Massachusetts, USA) at an accelerating voltage of 15 kV. The specimens were mounted on a carbon tape and sputter-coated with a layer of gold for 3 min, at 10^{-3}mbar and 10 mA current flow (SPI Supplies, Complete Sputter Coating System, West Chester, Pennsylvania, USA).

2.3.2. Particle size distribution

The dimensional characteristics and the particle size distribution of PHBH powders were investigated by means of Morphology 4 Instrument (Malvern Panalytical, Malvern, United Kingdom). This automatic morphological imaging analyzer was used to characterize individual particles within the powder. The analyses were carried out on a defined volume of dry powder of 5 mm^3 dispersed homogeneously on a glass plate, with a high-pressure dispersion of 4 bar and injection time of 10 ms. The sample volume is dependent on particle size and allows to have a representative view of the powder sample without overlapping particles. Pictures of the dispersed particles were then taken by the device. In this study, 10X magnification was used and only particles of diameter greater than 20 μm were considered in the analysis. In addition, to accurately define all the particles, the images were acquired by z-stacking six images of defocusing. This analysis applies the technique of automated static imaging with the purpose of providing a complete and detailed description of the morphological properties of the PHBH microspheres, in order to define and study their circularity, size, and shape.

2.3.3. Gas pycnometry

The true density (ρ) of the PHBH microspheres was determined using an Ultrapyc 5000 gas-pycnometer (Anton Paar GmbH, Graz, Austria) using helium as probe gas. Approximately 0.7 g of sample powder was placed in the 'small' sample cell, and the density was measured at 20 °C with the 'pulse' preparation mode and the 'fine powder' flow mode. A minimum of three passes and a final precision criterion of 0.01%, with three measurements per pass, were selected.

2.3.4. Microspheres flowability

The flowability of the PHBH microspheres was evaluated by determining the packing factor (φ), and the Hausner ratio (*HR*), by using a 100 mL graduated cylinder, according to a simplified method based on the ASTM D7481 standard [39]. φ and *HR* were calculated using Eqs. (1) and (2):

$$\varphi = \frac{\rho_{bulk}}{\rho} \tag{1}$$

$$HR = \frac{\rho_{tap}}{\rho_{bulk}} \tag{2}$$

where ρ_{bulk}, ρ, and ρ_{tap} are the apparent, the true and the tapped densities of the powder, respectively. Before each measurement, powders were oven-dried to overcome the influence of water absorbed onto the surface of the particles.

2.3.5. Differential scanning calorimetry

Thermal properties, such as melting and crystallization behavior of PHBH, were evaluated by differential scanning calorimetry (DSC) pre and post the microspheres fabrication. The samples were tested under N_2 flow of 40 mL/min, using a DSC 214 Polyma Equipment (Netzsch Group, Selb, Germany). The samples underwent a first heating cycle at 10 °C/min from 25° to 180 °C, followed by a cooling cycle at 10 °C/min to −30 °C. Then, the second heating cycle at 10 °C/min ended up at 180 °C. The degree of crystallization (X_c) was estimated by using Eq. (3):

$$X_c = \frac{\Delta H_m - \Delta H_{cc}}{\Delta H_m^0} \times 100 \tag{3}$$

where, ΔH_m, ΔH_{cc}, and ΔH_m^0 represent the enthalpy of melting, the enthalpy of cold crystallization and the enthalpy of fusion of fully crystalline PHBH (115 J/g) [40], respectively.

The first heating cycle was recorded in order to eliminate the thermal history of the samples. The thermal transitions of the pellets and microspheres were then measured on the cooling and the second heating cycles.

2.3.6. Thermogravimetric analysis (TGA)

Thermal stability of granules and powder was performed by thermogravimetric analysis (TGA) using a Mettler-Toledo TGA 851e instrument (Mettler Toledo, Columbus, Ohio, USA). The samples were heated from 25° to 600 °C with a heating rate of 10 °C/min under an airflow of 50 mL/min. All curves were normalized to the unit weight of the samples.

2.4. SLS 3D printing

3D-printed PHBH samples were manufactured using a Sharebot SnowWhite^2 SLS machine (Sharebot S.r.l., Nibionno, Italy) equipped with a CO_2 laser beam having a 14 W maximum power output and a

Table 1
Different experimental conditions for the oil-in-water (O/W) emulsion solvent evaporation method for PHBH microspheres fabrication.

Experimental condition	w/v concentration of PHBH in $CHCl_3$ (OIL PHASE) [%]	w/v concentration of PVA in H_2O (WATER PHASE) [%]	Ratio V_{OIL}:V_{WATER} [%]
EC1	5	1.00	15
EC2	5	0.20	15
EC3	15	0.50	25
EC4	10	0.50	25
EC5	7	0.25	15

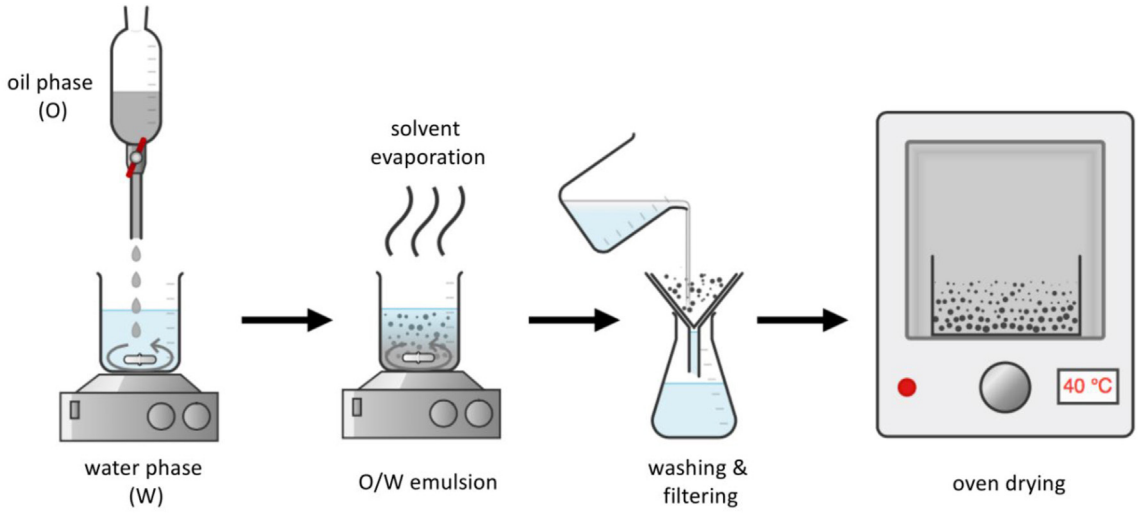

Fig. 1. Schematic representation of the manufacturing process for obtaining PHBH microspheres and its main steps of oil (PHBH + $CHCl_3$) in water (H_2O + PVA) emulsification, solvent evaporation, washing, filtering and drying. PHBH, poly(3-hydroxybutyrate-*co*-3-hydroxyhexanoate); PVA, poly (vinyl alcohol).

wavelength of 10.6 μm. Power is controlled as a percentage of its maximum output.

A value of 25% (3.5 W) was generally set for solid pieces, whereas 35% (4.9 W) is preferred for pieces with extremely thin walls and intricate structures. The laser power for the part perimeter has been set to a 5% increment with respect to the infill region. The polymer powder is distributed by a blade recoater in the presence of air during the printing process. The building chamber temperature was set at 90 °C.

Another important parameter was the laser scan speed, which is measured with respect to the machine resolution, in dots/s, which corresponds to 0.06 mm/s. This has generally been kept at default values (40,000 dots/s for the inner layers and 64,000 dots/s for the border). Three warming layers were used for the prints, i.e. spread for three consecutive layers, without any laser hatching. The selected parameters were 3.5 W laser power (P), 0.1 mm scan spacing (S_s), 2400 mm/s laser scan speed (v), 0.1 mm layer thickness (l), and 90 °C building chamber temperature (T_{bed}).

This setting resulted in a Volumetric Energy Density (VED) of 0.146 J/mm^3, where VED was calculated using Eq. (4) [41]:

$$VED = \frac{P}{S_s \cdot v \cdot l} \tag{4}$$

Once all process parameters were set in the desired range, the printer ramps up in steps until the targeted build chamber temperature is reached. A waiting time of 120–300 s was set after reaching the desired temperature, in order to obtain a uniformly heated powder bed.

2.5. Characterization of 3D-printed objects by SLS

2.5.1. Thermogravimetric analysis (TGA)

Thermal stability of the objects 3D-printed by SLS was evaluated by TGA using a Mettler-Toledo TGA 851e instrument (Mettler Toledo, Columbus, Ohio, USA). The samples were heated from 25° to 900 °C with a heating rate of 10 °C/min under an airflow of 50 mL/min. All curves were normalized to the unit weight of the samples.

2.5.2. Dynamic mechanical analysis

The dynamic mechanical analysis (DMA) of the 3D-printed biopolymeric objects was carried out with a Triton Technology Instrument on a sample of 10 layers. The instrument applied uniaxial tensile stress at a frequency of 1 Hz from −80 °C to 80 °C. The initial temperature of −80 °C was achieved by cooling down the test chamber with liquid nitrogen. The measurements were done to detect the elastic (E′) and viscous (E″) components of the modulus of the polymeric material, and the glass transition temperature (T_g) as the maximum of tan curve and were stopped after the rubbery plateau. For this analysis, the 3D-printed sample was rectangular and had the following dimensions: length (L) of 50 mm, width (W) of 10 mm, and thickness (T) of 1 mm.

3. Results and discussions

3.1. Morphological analyses

Thanks to scanning electron microscopy (SEM) microscopy, it was possible to validate or discard the distinct EC of the powder production processes. Comparing EC2 with EC1, the oil phase concentration (w/v_{OIL}) and emulsion ratio (V_{OIL}:V_{WATER}) were kept constant, while the water phase concentration (w/v_{WATER}) was decreased. From the morphological analysis, it can be observed that, in the EC2 case, the obtained powder had better spherical shape, which could facilitate the flowability and the spreadability, highly desirable features for powders to be used on SLS 3D printers.

Differently, to evaluate the effect of the oil phase concentration (w/v_{OIL}), the water phase concentration (w/v_{WATER}) as well as the emulsion ratio (V_{OIL}:V_{WATER}) remained unchanged for case studies EC3 and EC4, but the oil phase concentration was decreased from 15 to 10% w/v. Hence, it was noted that by reducing the concentration of PHBH in the organic solvent, and thus also the viscosity of the solution, the dripping process was facilitated, and the final size of the microspheres was consequently affected, reaching a smaller average particle size.

Eventually, it was set up an optimal parameter configuration (EC5) using a 7% w/v oil phase concentration, a 0.25% w/v water phase concentration, and a 15% emulsion ratio. For this fabrication parameter, the morphology of the PHBH powder was analyzed by SEM, and some significant results are presented in Figs. 2 (a) and (b).

From the analysis of these images, it is possible to observe that the biopolymer microspheres possess a regular spherical shape and a slightly wavy surface. From SEM image analysis, the mean

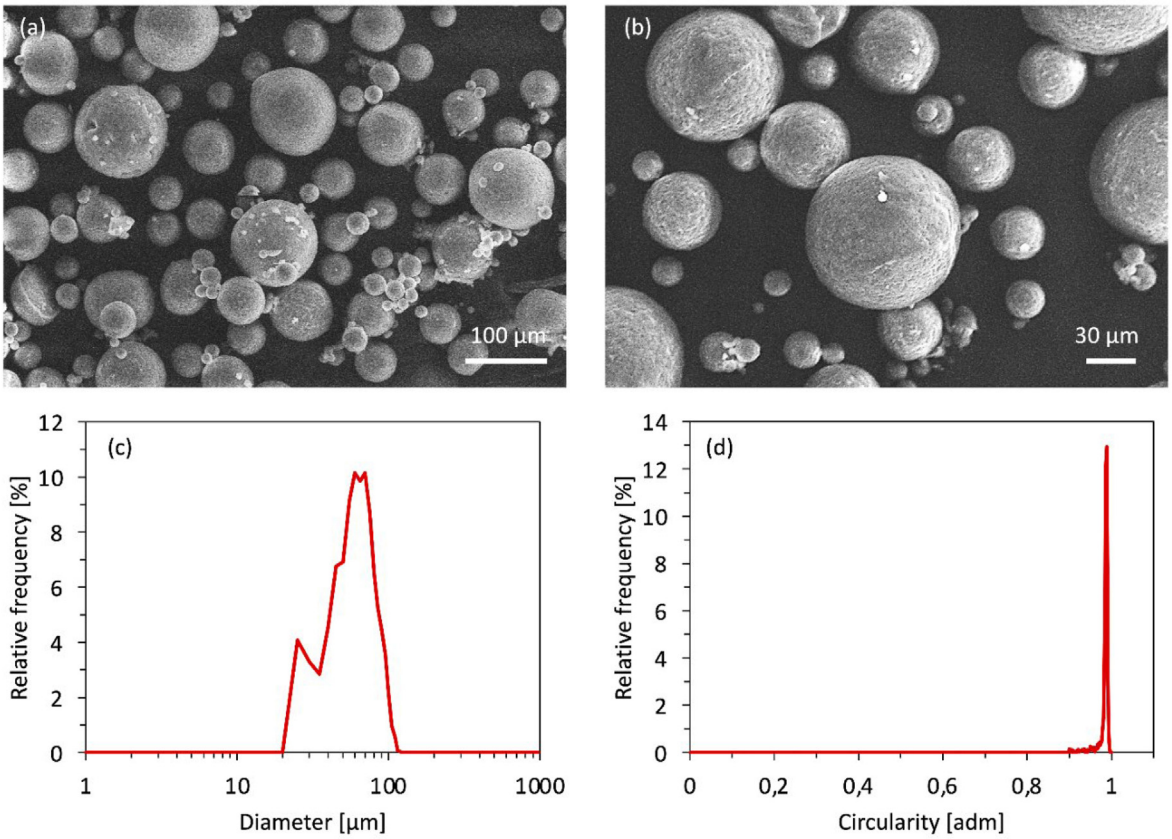

Fig. 2. SEM micrographs of PHBH microspheres obtained via emulsion solvent evaporation (EC5), at two different magnifications: (**a**) 280x and (**b**) 750x. PHBH microspheres size distribution (**c**), and circularity (**d**) obtained by morphological imaging analysis. PHBH, poly(3-hydroxybutyrate-*co*-3-hydroxyhexanoate); SEM, scanning electron microscopy.

diameter of the microspheres was calculated to be around 65 ± 33 µm. It is important to note that the size distribution of the obtained PHBH powders is in line with what was reported in previous papers as the desired powder size range for SLS processing [39]. Given the best morphological results for EC5, all further characterization and experimental steps were performed only on the microspheres obtained at these fabrication conditions.

Particle size distribution needs to be optimized for powders suitable for SLS process. In fact, as well-known from the literature, polymeric powders must fulfill a demanding combination of intrinsic and extrinsic properties to be processed by SLS, such as suitable size and shape. Specifically, SLS polymeric particles should be near-spherical in shape in order to encourage as free-flowing characteristics of the powders as possible and possess an optimal particle size range between 10 and 100 µm [42,43]. Thus, by combining particle size measurements such as length and width, with particle shape assessments such as circularity and convexity, the morphological imaging leads to obtain a fully characterization of spherical-shaped particles. In this case, statistically representative distributions were constructed by rapidly and automatically analyzing hundreds of thousands of particles per measurement, providing valuable information on the PHBH sample.

The particle size was directly measured dry, which best describes the status of the powder regarding its application during 3D printing. Each particle in the sample was measured individually in a relatively short time, providing high resolution and detailed information, which can be used as a complement to SEM investigations. Fig. 2 (c) shows the size distribution of PHBH microspheres. In particular, the PHBH microsphere D10, D50, and D90 values are 34.36 µm, 60.65 µm, and 86.05 µm, respectively. The D50 value gives the median of the distribution, while the D10 and D90 values indicate the distribution width. These results highlight that the PHBH particles size distribution approaches the ideal range as close as possible.

Moreover, the sphericity of the PHBH microspheres is also validated by the value of the circularity, which is close enough to 1, i.e. 0.98 ± 0.01, as shown in Fig. 2 (d). Besides, the values of convexity and elongation are approximately 1 and 0, respectively, guaranteeing an almost ideal spherical shape. These granulometry observations are significantly consistent with SEM investigation.

3.2. Determination of powder density

The density of the PHBH powder was characterized by a gas-pycnometer using helium, and after 15 measurements, an average real density of 1.21 ± 0.01 g/cm^3 was calculated, which coincides with the density declared in the PHBH pellet supplier datasheet. Therefore, it can be assumed that, regardless of the relatively rough surface morphology, the obtained microspheres are fully dense, which is a highly desired result for a good SLS printing process. Then, the packing and flowing behavior of the biopolymer powder was studied using tap density tests. According to previous studies, a HR value between 1 and 1.11 can be considered an indication of an excellent flow behavior [44], and this is precisely the case with our powders that present an HR of 1.06 ± 0.02 and a packing factor of 0.55. These results are consistent with SEM characterization, and a correlation between these data and the morphological and granulometric analysis is noteworthy. In fact, the regular and spherical morphology of the PHBH powder implies an almost free-flowing behavior, which in turn leads to homogeneous powder

spreadability on the SLS build platform by the recoating system, thus providing good predictions of 3D printability by SLS.

3.3. Thermal stability

The thermal characterization of polymer powders is of primary importance to better understand the behavior during the printing process and to obtain an indication of the printability. As a matter of fact, to define a proper powder bed temperature for semi-crystalline polymers, it is highly desirable to have a wide range between the melting (T_m^{onset}) and crystallization (T_c^{onset}) onset temperatures, referred to as sintering window. In this way, the sintering process can be guaranteed below the T_m, so avoiding undesired polymer melting or degradation. Besides, a large sintering window is favorable to delay the crystallization process as much as possible, thus preventing out-of-plane warping of the part [45]. Therefore, to have a deeper insight into PHBH thermal behavior and to establish suitable printing conditions, DSC and TGA analyzes were performed pre and post microspheres fabrication. Fig. 3 (a) shows the DSC results of PHBH pellet and PHBH powder (PHBH_p), and all DSC data are collected and presented in Table 2.

Independently from the microsphere fabrication process, PHBH displays glass transition temperature, crystallization, cold crystallization, and multiple melting phenomena. The bimodal melting behavior is typical of polyesters, and it is due to the presence of crystals that melt at T_{m1} and then reorganize into new crystals with higher structural perfection, which are more stable and that melt at a higher temperature, namely T_{m2} [46,47]. Moreover, noteworthy is the wide sintering window of this biopolymer, which was found to be 39 °C for PHBH pellets and even slightly increased, to 43 °C, for PHBH microspheres. This feature can be a favorable aspect for subsequent processability via SLS technique.

Fig. 3 (b) shows thermogravimetric curves of the PHBH pellet and powder. It can be easily observed that thermal stability is not affected by the microsphere fabrication via emulsion solvent evaporation. In fact, by evaluating the thermal stability at the temperatures associated with mass weight loss of 1 wt% ($T_{1wt.\%}$) and 10 wt% ($T_{10\ wt\%}$), a very slight increase in the temperatures is observed. The TGA curves for both PHBH samples, pellets and powder, have the same behavior. This suggests that the microsphere fabrication method does not have a significant effect on the final thermal properties of the biopolymer. At higher temperatures, a single-step degradation process occurs, at around 300 °C, both for pellet and powder, resulting in more than 99% of PHBH decomposing, as also shown by the DTG curve. It can be concluded that the PHBH powder shows no thermal degradation close to the printing temperature region, suggesting that the powder can withstand the applied heating without degrading, and thus a temperature of about 95 °C seems to be an excellent value of pre-heating temperature for the bed powder.

3.4. 3D printing process by SLS

In order to study the 3D printability of PHBH by SLS, simple monolayer geometries with increasing internal complexity, such as a square, a square with 4 symmetrical holes and a hexagon with an intricate internal pattern were first realized, as reported in Fig. 4 (a). Subsequently, the possibility to develop in the z-direction was assessed by the fabrication of prisms with a rectangular base and a number of layers varying from 5 to 15, as can be observed in Fig. 4 (b). Geometries with a more complicated internal structure, given by the close alternation of full and empty spaces and the circular shapes of the holes, as well as a more significant vertical development, were also realized, leading to the fabrication of a subsequent deposition of 50 layers as clearly shown in Fig. 4 (c).

3.5. Thermal and DMA of 3D-printed samples

The TGA of 3D-printed samples was carried out in oxidizing atmosphere, in order to get a complete thermal characterization of the PHBH after the 3D-printing SLS process. The TGA and DTG curves of a 3D-printed 10 layers PHBH sample are reported in Fig. 5 (a). The thermal degradation of the PHBH sample in air occurs with a maximum decomposition rate temperature at around 298 °C. This result reveals that the laser printing process had no effect on the final thermal stability of the 3D-printed samples. As previously shown, the curve is comparable with those of the PHBH pellet and powder, respectively.

The viscoelastic characterization of the 3D-printed object of 10 layers obtained by SLS was also performed by means of DMA

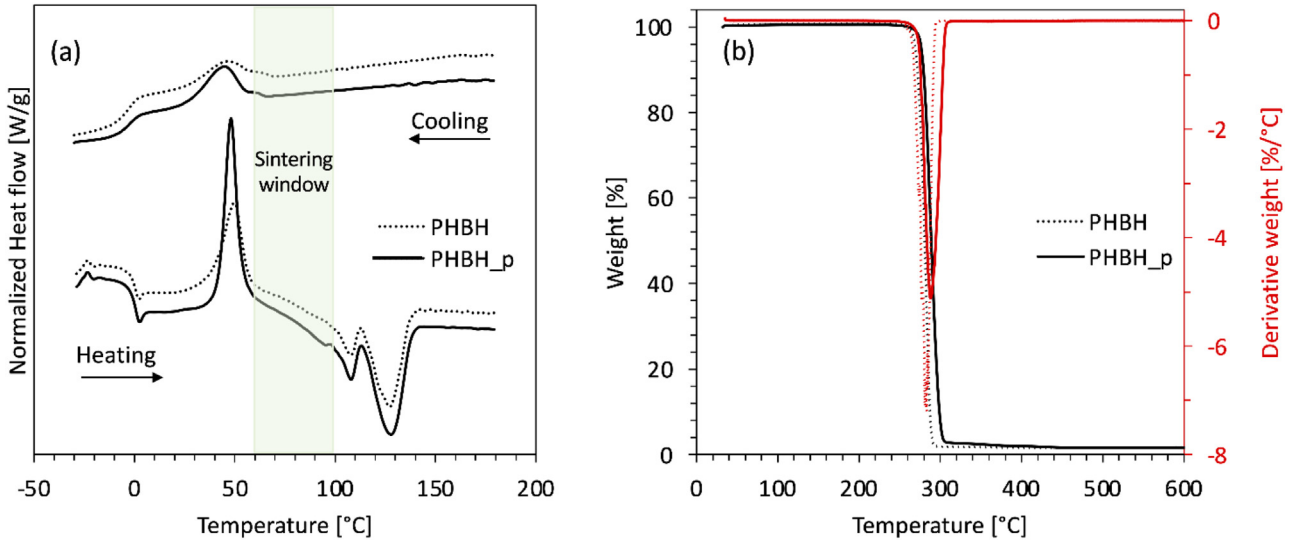

Fig. 3. Thermal characterization of PHBH pellet (PHBH), PHBH powder (PHBH_p) obtained via emulsion solvent evaporation. (**a**) DSC scans during heating and cooling cycles from −30 to 180 °C (Exo Up). (**b**) TGA and DTG curves of the samples tested from 25° to 600 °C under air flow. PHBH, poly(3-hydroxybutyrate-*co*-3-hydroxyhexanoate); DSC, differential scanning calorimetry; TGA, thermogravimetric analysis.

Table 2
Thermal transition temperatures and enthalpies of PHBH as pellet and microspheres, obtained by DSC analysis under an inert atmosphere.

	Cooling		Heating								
	ΔH_c [J/g]	T_c^{onset} [°C]	T_g [°C]	T_{cc}^{peak} [°C]	ΔH_{cc} [J/g]	ΔH_m [J/g]	T_{m1}^{onset} [°C]	T_{m1}^{peak} [°C]	T_{m2}^{onset} [°C]	T_{m2}^{peak} [°C]	X_c [%]
PHBH	9.7	63.2	−0.6	48.0	35.3	51.1	101.8	107.8	112.4	127.8	13.7
PHBH_p	12.8	56.9	−0.4	49.5	26.1	43.2	100.4	107.8	114.7	127.3	14.8

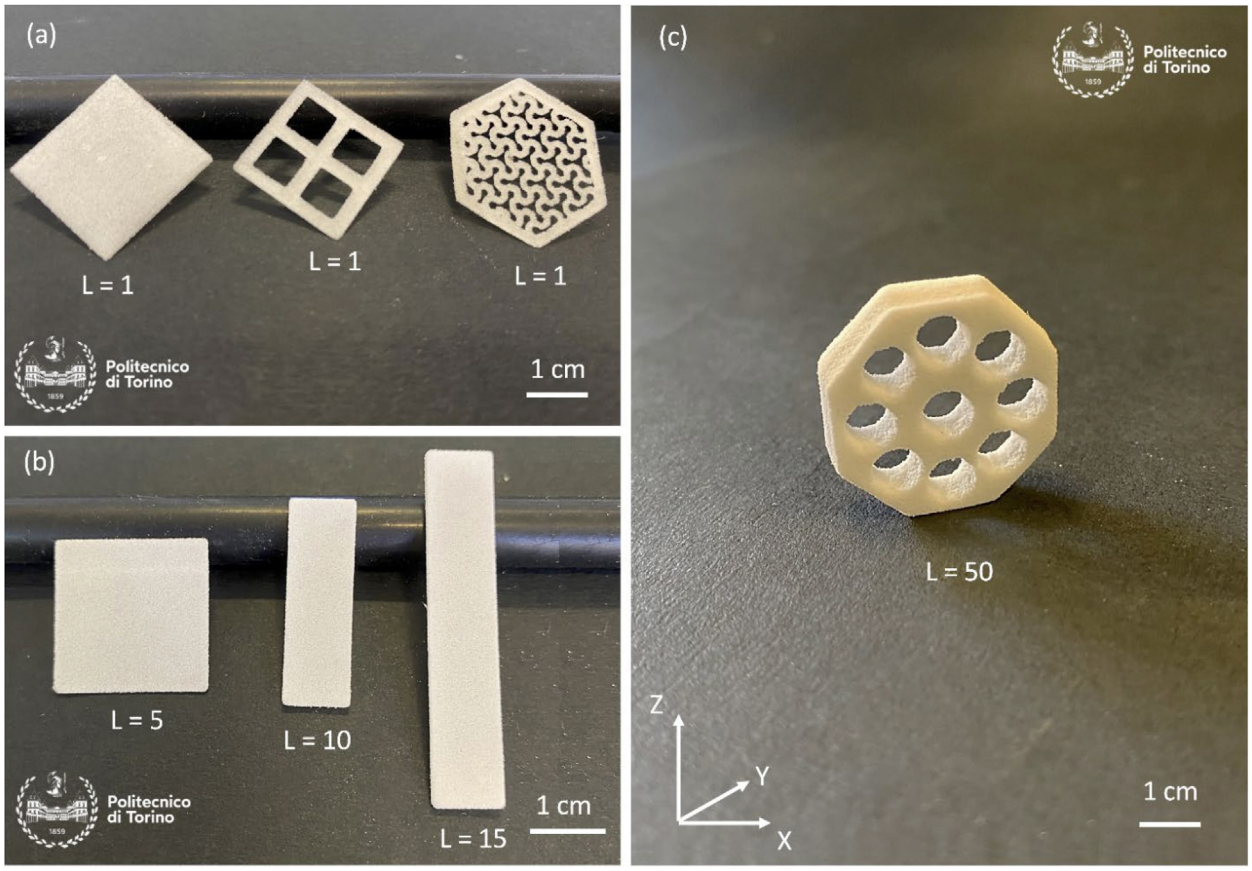

Fig. 4. Representative view of 3D-printed geometries obtained by SLS starting from PHBH microspheres, at different number of layers (L): (**a**) monolayer geometries, (**b**) multilayers geometries, and (**c**) complex-shaped structure. PHBH, poly(3-hydroxybutyrate-*co*-3-hydroxyhexanoate); SLS, selective laser sintering.

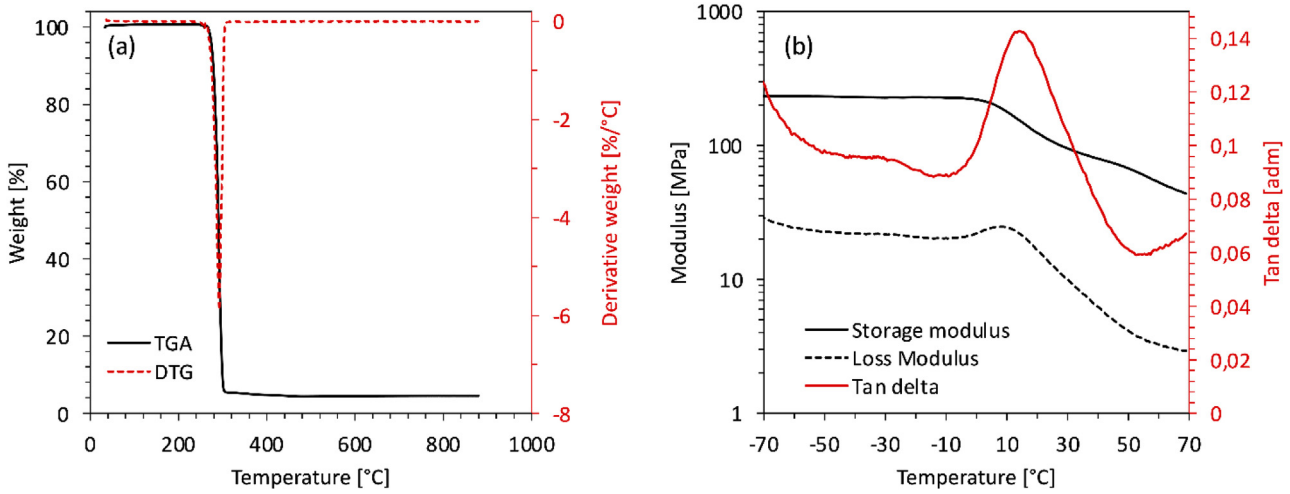

Fig. 5. Thermogravimetric analysis (TGA) and dynamic mechanical analysis (DMA) of a 3D-printed sample of 10 layers of PHBH obtained by SLS. PHBH, poly(3-hydroxybutyrate-*co*-3-hydroxyhexanoate); SLS, selective layer sintering.

analysis. While DSC analysis gives information about the thermal behavior, DMA allows the measure of storage (E′) and loss (E″) moduli and the evaluation of tan δ as E″/E′ ratio. This technique gives a complete characterization of the thermal and viscoelastic properties of the polymeric material. Fig. 5 (b) reports the tan δ curve, from which is possible to evaluate the glass transition temperature of the PHBH. It can be observed that the T_g value, taken as the maximum of the tan δ curve, is at 14 °C, a higher value with respect to that obtained from DSC analysis. This behavior, already previously observed in literature, can be attributed to a frequency effect [47]. In fact, while DSC is sensitive to the heat capacity (C_p) changes associated with the glass transition, DMA is sensitive to a mechanical relaxation, also associated with the glass transition, and the expression of this strictly depends on the mechanical frequency imposed by the test. Fig. 5 (b) shows the storage (233 MPa) and loss (23 MPa) moduli evaluated at −50 °C on a rectangular 3D-printed object of 10 layers obtained by SLS.

Comparing these results with the previous findings in the literature, it can be observed that the storage and loss modulus values for PHBH are lower than those of the traditional fossil-based thermoplastic polymers used for SLS applications, such as polyamides.

For example, Salmoria et al. calculated a storage modulus, in the glassy plateau, of 650 MPa and 1100 MPa for PA6 and PA12, respectively [48]. The DMA results are in good agreement with the low mechanical performance of biopolymers [49]. Tailoring of the mechanical properties of PHBH is needed to use it as an alternative to the common thermoplastic polymers in a wide range of applications, contributing to solve the pollution issue thanks to its excellent biodegradability and sustainability.

4. Conclusions

In this research work, the production of PHBH powder with spherical shape and size lower than 100 μm was the first step carried out. The obtained powder was used to prove the 3D printability by SLS of this innovative, fully bio-based, and biodegradable polymer. The manufacturing procedure followed to obtain the microspheres was an oil-in-water emulsion solvent evaporation method. The biopolymeric microspheres obtained showed specific particle size and sphericity useful to be processed by AM. The biopolymer powder was characterized according to the morphology, the flowing behavior, and thermal stability, and all the results suggested a proper sinterability of the bio-based material. The fabricated PHBH powder was finally used as feedstock for an SLS printer, denoting proper and successful 3D printability. In addition, the obtained samples showed good thermal stability and interesting dynamic mechanical performance. Therefore, the presented approach seems to be an attractive candidate for SLS applications.

This study certainly deserves further investigation to evaluate the scalability of the microsphere fabrication process, as well as to optimize the printing process to achieve even more complex 3D architectures. Besides, an important aspect to be addressed in future developments of this project is to try to reduce the environmental footprint of this fabrication process by considering possible strategies for the recovery of organic solvents, such as could be the recondensation of chloroform during evaporation. This aspect was not considered in this first paper because it was beyond the scope of this preliminary research, which aimed to evaluate the applicability of PHBH for SLS and the characterization of the final 3D-printed samples.

However, this preliminary research work opens up interesting future scenarios for novel applications of this biopolymer. The possible fields of application of PHBH can be various and, of particular interest for the authors, could be the biomedical field.

In this case, the customization of medical devices, achieved through an AM approach, could also be valorized and enhanced by the use of bio-based, biodegradable, and biocompatible polymers, thus suggesting innovative tissue regeneration solutions.

Declaration of competing interest

The authors declare that they have no known competing financial interests or personal relationships that could have appeared to influence the work reported in this paper.

Data availability

Data will be made available on request.

References

[1] G. Rasiya, A. Shukla, K. Saran, Additive manufacturing-A review, Mater. Today Proc. 47 (2021) 6896–6901, https://doi.org/10.1016/j.matpr.2021.05.181.
[2] A. Alfaify, M. Saleh, F.M. Abdullah, A.M. Al-Ahmari, Design for additive manufacturing: a systematic review, Sustainability 12 (19) (2020) 7936–7957, https://doi.org/10.3390/su12197936.
[3] A. Merulla, A. Gatto, E. Bassoli, S.I. Munteanu, B. Gheorghiu, M.A. Pop, T. Bedo, D. Munteanu, Weight reduction by topology optimization of an engine subframe mount, designed for additive manufacturing production, Mater. Today Proc. 19 (2019) 1014–1018, https://doi.org/10.1016/j.matpr.2019.08.015.
[4] M. Khorram Niaki, F. Nonino, G. Palombi, S.A. Torabi, Economic sustainability of additive manufacturing, J. Manuf. Technol. Manag. 30 (2019) 353–365, https://doi.org/10.1108/JMTM-05-2018-0131.
[5] J. Fornaziero de Almeida, M. Neves Mourarias, M. Cecílio Gerolamo, R. Teixeira Coelho, The implementation of additive manufacturing (AM) in industries starting from the identification of organizational cultural characteristics - a review, International Journal of Engineering Materials and Manufacture 6 (2021) 242–258, https://doi.org/10.26776/ijemm.06.04.2021.02.
[6] KBV Research, Global additive manufacturing market size, share & industry trends analysis report by printer type, by technology, by component, by application, by material, by vertical by regional outlook and forecast, 2022 – 2028, 2022, 0–450.
[7] A. Xu, B. Langefeld, M. Erharter, V. Kourkejian, Market, Machines and Materials – the New Playground for Large Chemical Companies, 2020.
[8] N. Li, S. Huang, G. Zhang, R. Qin, W. Liu, H. Xiong, G. Shi, J. Blackburn, Progress in additive manufacturing on new materials: a review, J. Mater. Sci. Technol. 35 (2019) 242–269, https://doi.org/10.1016/j.jmst.2018.09.002.
[9] P. Minetola, F. Calignano, M. Galati, Comparing geometric tolerance capabilities of additive manufacturing systems for polymers, Addit. Manuf. 32 (2020), 101103, https://doi.org/10.1016/j.addma.2020.101103.
[10] A. Jaisingh Sheoran, H. Kumar, Fused Deposition modeling process parameters optimization and effect on mechanical properties and part quality: review and reflection on present research, Mater. Today Proc. 21 (2020) 1659–1672, https://doi.org/10.1016/j.matpr.2019.11.296.
[11] I. Baturynska, O. Semeniuta, K. Martinsen, Optimization of process parameters for powder bed fusion additive manufacturing by combination of machine learning and finite element method: a conceptual framework, Procedia CIRP 67 (2018) 227–232, https://doi.org/10.1016/j.procir.2017.12.204.
[12] X. Gao, S. Qi, X. Kuang, Y. Su, J. Li, D. Wang, Fused filament fabrication of polymer materials: a review of interlayer bond, Addit. Manuf. 37 (2021), 101658, https://doi.org/10.1016/j.addma.2020.101658.
[13] S.D. Nath, S. Nilufar, An overview of additive manufacturing of polymers and associated composites, Polymers 12 (2020) 2719–2751, https://doi.org/10.3390/polym12112719.
[14] F. Lupone, E. Padovano, F. Casamento, C. Badini, Process phenomena and material properties in selective laser sintering of polymers: a review, Materials 15 (2022) 183–219, https://doi.org/10.3390/ma15010183.
[15] Y. Wang, Z. Xu, D. Wu, J. Bai, Current status and prospects of polymer powder 3D printing technologies, Materials 13 (10) (2020) 2406, https://doi.org/10.3390/ma13102406.
[16] M.A. Dechet, A. Goblirsch, S. Romeis, M. Zhao, F.J. Lanyi, J. Kaschta, D.W. Schubert, D. Drummer, W. Peukert, J. Schmidt, Production of polyamide 11 microparticles for Additive Manufacturing by liquid-liquid phase separation and precipitation, Chem. Eng. Sci. 197 (2019) 11–25, https://doi.org/10.1016/j.ces.2018.11.051.
[17] T. Heckner, M. Seitz, S.R. Raisch, G. Huelder, P. Middendorf, Selective laser sintering of pa6: effect of powder recoating on fibre orientation, Journal of Composites Science 4 (2020) 108–123, https://doi.org/10.3390/jcs4030108.
[18] P.C. Gomes, O.G. Piñeiro, A.C. Alves, O.S. Carneiro, On the reuse of SLS polyamide 12 powder, Materials 15 (2022) 5486–5501, https://doi.org/10.3390/ma15165486.

[19] W. Han, L. Kong, M. Xu, Advances in selective laser sintering of polymers, Int. J. Extrem. Manuf. 4 (2022), 042002. http://iopscience.iop.org/article/10.1088/2631-7990/ac9096.
[20] J. Li, W. Wu, X. Zhang, T. Zhao, Z. Wang, S. Li, Effect of layered double hydroxide on the flame retardancy of intumescent flame retardant thermoplastic polyurethane composites prepared by selective laser sintering, J. Appl. Polym. Sci. 139 (2022), 52838, https://doi.org/10.1002/app.52838.
[21] Data Bridge Market Research, Global Selective Laser Sintering Equipment Market – Industry Trends and Forecast to 2029, 2022.
[22] J. Nikiema, Z. Asiedu, A review of the cost and effectiveness of solutions to address plastic pollution, Environ. Sci. Pollut. Control Ser. 29 (2022) 24547–24573, https://doi.org/10.1007/s11356-021-18038-5.
[23] K.L. Law, R. Narayan, Reducing environmental plastic pollution by designing polymer materials for managed end-of-life, Nat. Rev. Mater. 7 (2022) 104–116, https://doi.org/10.1038/s41578-021-00382-0.
[24] Nova-Institute, Bio-based Building Blocks and Polymers, 2020.
[25] J. Baranwal, B. Barse, A. Fais, G.L. Delogu, A. Kumar, Biopolymer: a sustainable material for food and medical applications, Polymers (Basel) 14 (2022) 983–1004, https://doi.org/10.3390/polym14050983.
[26] M.Y. Khalid, Z.U. Arif, Novel biopolymer-based sustainable composites for food packaging applications: a narrative review, Food Packag. Shelf Life 33 (2022), 100892, https://doi.org/10.1016/j.fpsl.2022.100892.
[27] C. Sciancalepore, E. Togliatti, A. Giubilini, D. Pugliese, | Fabrizio Moroni, M. Messori, D. Milanese, Preparation and characterization of innovative poly (butylene adipate terephthalate)-based biocomposites for agri-food packaging application, J. Appl. Polym. Sci. 139 (2022) 52370–52387, https://doi.org/10.1002/app.52370.
[28] A. Jahandideh, M. Ashkani, N. Moini, Chapter 8 - biopolymers in textile industries, in: S. Thomas, S. Gopi, A. Amalraj (Eds.), Biopolymers and Their Industrial Applications, Elsevier, 2021, pp. 193–218, https://doi.org/10.1016/B978-0-12-819240-5.00008-0.
[29] S. Sundharamurthi, T.R. Sreeraj, A. Amalraj, S. Gopi, Chapter 13 - biopolymer composites in supercapacitor and energy storage devices, in: S. Thomas, S. Gopi, A. Amalraj (Eds.), Biopolymers and Their Industrial Applications, Elsevier, 2021, pp. 305–329, https://doi.org/10.1016/B978-0-12-819240-5.00013-4.
[30] C. Cui, Q. Fu, L. Meng, S. Hao, R. Dai, J. Yang, Recent progress in natural biopolymers conductive hydrogels for flexible wearable sensors and energy devices: materials, structures, and performance, ACS Appl. Bio Mater. 4 (2021) 85–121, https://doi.org/10.1021/acsabm.0c00807.
[31] A. Giubilini, F. Bondioli, M. Messori, G. Nyström, G. Siqueira, Advantages of additive manufacturing for biomedical applications of polyhydroxyalkanoates, Bioengineering 8 (2) (2021) 29–59, https://doi.org/10.3390/bioengineering8020029.
[32] A. Nobili, V. Volpini, A. Giubilini, L. Corsi, F. Bondioli, Characterization of biocompatible scaffolds manufactured by fused filament fabrication of poly(3-hydroxybutyrate-co-3-hydroxyhexanoate), R. Soc Open Sci 9 (4) (2022), 211485, https://doi.org/10.1098/rsos.211485.
[33] K. Eraslan, C. Aversa, M. Nofar, M. Barletta, A. Gisario, R. Salehiyan, Y. Alkan Goksu, Poly(3-hydroxybutyrate-co-3-hydroxyhexanoate) (PHBH): synthesis, properties, and applications-A review, Eur. Polym. J. 167 (2022) 111044–111058.
[34] B. Duan, M. Wang, Encapsulation and release of biomolecules from Ca–P/PHBV nanocomposite microspheres and three-dimensional scaffolds fabricated by selective laser sintering, Polym. Degrad. Stabil. 95 (2010) 1655–1664, https://doi.org/10.1016/j.polymdegradstab.2010.05.022.
[35] M. Gómez-Cerezo, R. Patel, C. Vaquette, L. Grøndahl, M. Lu, In vitro evaluation of porous poly(hydroxybutyrate-co-hydroxyvalerate)/akermanite composite scaffolds manufactured using selective laser sintering, Biomaterials Advances 135 (2022), 212748.
[36] S.H. Diermann, M. Lu, M. Dargusch, L. Grøndahl, H. Huang, Akermanite reinforced PHBV scaffolds manufactured using selective laser sintering, J. Biomed. Mater. Res. B Appl. Biomater. 107 (8) (2019) 2596–2610.
[37] S.H. Diermann, M. Lu, Y. Zhao, M. Dargusch, H. Synthesis Huang, microstructure, and mechanical behaviour of a unique porous PHBV scaffold manufactured using selective laser sintering, J. Mech. Behav. Biomed. Mater. 84 (2018) 151–160.
[38] R. Patel, D. Monticone, M. Lu, L. Grøndahl, H. Huang, Hydrolytic degradation of porous poly(hydroxybutyrate-co-hydroxyvalerate) scaffolds manufactured using selective laser sintering, Polym. Degrad. Stabil. 187 (2021), 109545, https://doi.org/10.1016/j.polymdegradstab.2021.109545.
[39] M. Schmid, F. Amado, G. Levy, K. Wegener, Flowability of powders for selective laser sintering (SLS) investigated by round robin test, in: High Value Manufacturing: Advanced Research in Virtual and Rapid Prototyping - Proceedings of the 6th International Conference on Advanced Research and Rapid Prototyping, VR@P 2013, 2014, pp. 95–99. https://www.scopus.com/inward/record.uri?eid=2s2.084892186734&partnerID=40&md5=1eb82e94c65fa5fb6fccc5d27c130d1b.
[40] D. Li, J. Zhou, X. Ma, J. Li, Synthesis of a novel biocomposite of poly (3-hydroxybutyrate-co-3-hydroxyhexanoate) reinforced with acetylated cellulose nanocrystals, Cellulose 26 (2019) 8729–8743, https://doi.org/10.1007/s10570-019-02708-2.
[41] M. Schmid, K. Wegener, Additive manufacturing: polymers applicable for laser sintering (LS), Procedia Eng. 149 (2016) 457–464, https://doi.org/10.1016/j.proeng.2016.06.692.
[42] J. Schmidt, M. Sachs, C. Blümel, B. Winzer, F. Toni, K.-E. Wirth, W. Peukert, A novel process chain for the production of spherical SLS polymer powders with good flowability, Procedia Eng. 102 (2015) 550–556, https://doi.org/10.1016/j.proeng.2015.01.123.
[43] Mwania Fredrick Mulinge, Maringa Maina, G. van der Walt Jacobus, A review of the techniques used to characterize laser sintering of polymeric powders for use and re-use in additive manufacturing, Manuf. Rev. 8 (2021) 14–30, https://doi.org/10.1051/mfreview/2021012.
[44] A.T. Sutton, C.S. Kriewall, M.C. Leu, J.W. Newkirk, Powder characterisation techniques and effects of powder characteristics on part properties in powder-bed fusion processes, Virtual Phys. Prototyp. 12 (2017) 3–29, https://doi.org/10.1080/17452759.2016.1250605.
[45] A.D. Valino, J.R.C. Dizon, A.H. Espera, Q. Chen, J. Messman, R.C. Advincula, Advances in 3D printing of thermoplastic polymer composites and nanocomposites, Prog. Polym. Sci. 98 (2019), 101162, https://doi.org/10.1016/j.progpolymsci.2019.101162.
[46] D. Jonnalagadda, T. Kuboki, Effect of natural flours on crystallization behaviors of poly(3-hydroxybutyrate-co-3-hydroxyhexanoate), J. Appl. Polym. Sci. 133 (2016), 43600, https://doi.org/10.1002/app.43600.
[47] A. Kovalcik, Recent advances in 3D printing of polyhydroxyalkanoates: a review, Eurobiotech J 5 (2021) 48–55, https://doi.org/10.2478/ebtj-2021-0008.
[48] G. v Salmoria, J.L. Leite, L.F. Vieira, A.T.N. Pires, C.R.M. Roesler, Mechanical properties of PA6/PA12 blend specimens prepared by selective laser sintering, Polym. Test. 31 (2012) 411–416, https://doi.org/10.1016/j.polymertesting.2011.12.006.
[49] C.A. Gracia-Fernández, S. Gómez-Barreiro, J. López-Beceiro, J. Tarrío Saavedra, S. Naya, R. Artiaga, Comparative study of the dynamic glass transition temperature by DMA and TMDSC, Polym. Test. 29 (2010) 1002–1006, https://doi.org/10.1016/j.polymertesting.2010.09.005.